

Project Report  
ATC-455

# WSR-88D Microburst Detection Performance Evaluation

J.Y.N. Cho  
B.J. Bennett

28 November 2023

---

**Lincoln Laboratory**  
MASSACHUSETTS INSTITUTE OF TECHNOLOGY  
*LEXINGTON, MASSACHUSETTS*



---

This material is based upon work supported by the Federal  
Aviation Administration under Air Force Contract No.  
FA8702-15-D-0001.

DISTRIBUTION STATEMENT A. Approved for public  
release. Distribution is unlimited.

This report is the result of studies performed at Lincoln Laboratory, a federally funded research and development center operated by Massachusetts Institute of Technology. This material is based upon work supported by the Federal Aviation Administration under Air Force Contract No. FA8702-15-D-0001. Any opinions, findings, conclusions or recommendations expressed in this material are those of the author(s) and do not necessarily reflect the views of the Federal Aviation Administration.

© 2023 Massachusetts Institute of Technology

Delivered to the U.S. Government with Unlimited Rights, as defined in DFARS Part 252.227-7013 or 7014 (Feb 2014). Notwithstanding any copyright notice, U.S. Government rights in this work are defined by DFARS 252.227-7013 or DFARS 252.227-7014 as detailed above. Use of this work other than as specifically authorized by the U.S. Government may violate any copyrights that exist in this work.

Massachusetts Institute of Technology  
Lincoln Laboratory

WSR-88D Microburst Detection Performance Evaluation

*J.Y.N. Cho*  
*B.J. Bennett*  
*Group 43*

Project Report ATC-455  
28 November 2023

DISTRIBUTION STATEMENT A. Approved for public release. Distribution is unlimited.

Lexington

Massachusetts

**This page intentionally left blank.**

## ABSTRACT

An empirical study of Weather Surveillance Radar 1988-Doppler (WSR-88D) microburst detection performance is conducted using Integrated Terminal Weather System (ITWS) microburst detections as reference. Data from 14 airport regions during 181 independent time periods spanning the years 2015–2022 are utilized for the evaluation. Results show that the detection and false alarm probabilities depend on event range from the WSR-88D. ITWS-level detection (~95%) and false alarm (~5%) probabilities are achieved for 0 to 20 km range, while at 20 to 30 km range, detection (~80%) and false alarm (~5%) rates meeting or exceeding Weather Systems Processor (WSP) microburst detection ( $\geq 80\%$ ) and false alarm ( $\leq 15\%$ ) probability requirements are observed. Beyond ~30 km from the radar, the WSR-88D microburst detection performance falls to operationally unacceptable levels.

Timing analysis indicates that, on average, WSR-88D microburst detections lag ITWS microburst detections with a median value on the order of 30 s. The detection time difference distribution shows a normal symmetric form around zero with a thin tail extending in the positive lag direction, implying that the thin tail is responsible for the positive median lag time. The lag distribution tail is shown to be shortened, and the median lag time reduced to ~10 s, if the WSR-88D's slower base scan update modes are eliminated.

The study shows that the WSR-88D (and its future replacement) could generate operationally useful microburst alerts for airports that are located close enough (less than ~20 km) to the radar. The long detection lag times for a small fraction of cases that are associated with WSR-88D scan strategies that have long base (lowest elevation angle) scan update periods is an issue that may need to be addressed if the current system is to be considered for operational air traffic control purposes. Also, the unavailability of output data from the first eight range gates (2 km) should be addressed for a future replacement radar by adding a minimum observation range requirement comparable to the Terminal Doppler Weather Radar's (TDWR; 0.5 km) to the follow-on radar program requirements.

**This page intentionally left blank.**

## TABLE OF CONTENTS

	<b>Page</b>
Abstract	iii
List of Illustrations	vii
List of Tables	ix
1. INTRODUCTION	1
2. METHODOLOGY	3
2.1 Locations	4
2.2 Event Search Process	5
2.3 Geometric Considerations	5
2.4 Detections vs. Events	6
2.5 Scoring Procedure	7
3. RESULTS	13
4. SUMMARY DISCUSSION	21
APPENDIX A: DATA LIST	23
Acknowledgments	29
Glossary	31
References	33

**This page intentionally left blank.**

## LIST OF ILLUSTRATIONS

<b>Figure No.</b>		<b>Page</b>
1	Framework for WSR-88D microburst detection performance assessment.	4
2	Illustration of the ITWS microburst detection merging process that results in an aggregate microburst event.	7
3	Microburst detection and lowest elevation angle radial velocity for WSR-88D (left) and ITWS (right) at Denver. White areas indicate invalid (censored) data. The airport reference point is denoted by the black dot in the center. The WSR-88D is located at the “N” and the TDWR is sited at the “T.” The scoring area (20 km from the airport and within microburst product output range of the WSR-88D and ITWS) is bounded by the black dashed line. The microburst $\Delta V$ values ( $\text{m s}^{-1}$ ) are shown inside the microburst polygons. See main text for further details.	10
4	Histogram of WSR-88D base scan update period at the times of microburst detection, missed detection, and false alarm for the 0–30-km radar-to-event range category.	16
5	Histogram of $T_{\text{lag}}$ for the 0–30-km WSR-88D-to-event range category.	17
6	Histogram of $T_{\text{lag}}$ for the 0–30-km WSR-88D-to-event range category and WSR-88D base scan update period less than or equal to 120 s.	17
7	Histogram of $T_{\text{lag}}$ for the 0–30-km WSR-88D-to-event range category and WSR-88D base scan update period greater than or equal to 240 s.	18

**This page intentionally left blank.**

## LIST OF TABLES

<b>Table No.</b>		<b>Page</b>
1	List of Airports Considered in Study	4
2	WSR-88D AMDA Performance	13
3	Wind-Shear Detection Performance Requirements	14
4	WSR-88D Data Periods Used in Study	23

**This page intentionally left blank.**

# 1. INTRODUCTION

Low-level wind shear, in particular a microburst, is a hazard to airport takeoff and landing operations. A series of fatal commercial airliner accidents in the 1970s and 1980s made this painfully clear, and, in response, ground-based sensors specifically designed to detect low-altitude wind shear were developed and deployed at many U.S. airports (McCarthy et al. 2022). There have been no documented commercial airline accidents attributed to wind shear at any of the airports serviced by these sensors since they have been operational.

Currently, there are 129 airport wind-shear detection systems in the U.S., composed of 45 Terminal Doppler Weather Radars (TDWRs; Michelson et al. 1990; Cho and Weber 2010), 34 Airport Surveillance Radar-9 Weather Systems Processors (ASR-9 WSPs; Weber and Stone 1994; Cho 2015), 49 Low-Level Wind-Shear Alert Systems (LLWASs; Wilson and Gramzow 1991), and one WindTracer lidar (Gatt et al. 2015). Eight LLWASs are co-located with TDWRs, the lidar is co-located with a TDWR, and one TDWR services two airports. Thus, 120 U.S. airports are served by one or more of these wind-shear detection systems. Because these systems have varying levels of detection coverage, performance, and cost, their deployment scheme was, in part, based on a cost/benefit analysis that took into account factors such as hazard exposure probability and airport traffic density (Martin Marietta 1994).

A more recent cost/benefit study considered the possibility that the tri-agency Weather Surveillance Radar 1988-Doppler (WSR-88D) might also be able to provide wind-shear detection services at some airports (Hallowell et al. 2009). (The WSR-88D is commonly known as the Next-Generation Weather Radar, or NEXRAD.) Indeed, their detection performance model showed that such a scenario was technically plausible (Cho and Hallowell 2008). In fact, the machine-intelligent gust front algorithm (MIGFA), which was originally developed for the ASR-9 WSP and TDWR (Troxel and Delanoy 1994), was adapted for (Smalley et al. 2005) and operationally deployed on the WSR-88D Open Radar Product Generator (ORPG) in 2008. Subsequently, the automated microburst detection algorithm (AMDA), which was first developed for the ASR-9 WSP (Newell and Cullen 1993), was adapted for and operationally deployed on the WSR-88D ORPG in 2015. Early pre-operational testing of AMDA showed very promising results on Denver, Colorado WSR-88D data (Veillette et al. 2013), as did a limited assessment conducted on 20 microburst cases (Wang et al. 2019).

Despite the favorable outcomes of these previous performance evaluations, the WSR-88D microburst and gust front detection products are generally not relied upon operationally by air traffic control (ATC) personnel. Unlike the official wind-shear alert products generated from TDWR, ASR-9 WSP, LLWAS, and lidar data, the WSR-88D wind-shear products are not shown on dedicated ribbon displays in airport control towers. There are still concerns about the reliability and timeliness of the WSR-88D wind-shear alerts due to several factors: (1) unlike the TDWRs, which were optimally located for airport microburst detection, WSR-88Ds were sited to serve multiple purposes, such as hazardous weather prediction for highly populated areas and efficient nationwide coverage (Leone et al. 1989). (2) Also, unlike the TDWR, which

has an automated volume scan strategy that is optimized for microburst detection, the WSR-88D is a tri-agency system controlled by National Weather Service (NWS) weather forecast office (WFO) radar operators who make scan strategy decisions based on their various competing needs. (3) Relative to the TDWR, the WSR-88D has coarser range resolution (250 m vs. 150 m) and a less sharp focus in the vertical dimension ( $1^\circ$  vs.  $0.5^\circ$  elevation beamwidth). (4) Finally, the signal-to-clutter ratio (SCR) for distributed ground clutter tends to be lower at S band relative to C band (Evans and Turnbull 1989).

Note, however, that the WSR-88D has much better vertical and azimuthal resolution and sensitivity compared to the ASR-9 WSP (Cho et al. 2013), as well as smaller reflectivity and velocity estimation errors thanks to the longer dwell times. Operation at S band holds some advantages over C band, such as less range-velocity ambiguity (Cho et al. 2013), signal attenuation, and radio frequency (RF) interference (Saltikoff et al. 2016). In fact, the early TDWR prototype was an S-band radar, which provided excellent wind-shear detection capability, and the switch to C band had to be validated with respect to detection performance prior to operational system production (Evans and Bernella 1994). (The transition to C band was largely necessitated by the lack of RF spectrum availability near airports due to the incumbent S-band ASRs.) Furthermore, the WSR-88D has dual polarization, which the TDWR and ASR-9 WSP do not, although AMDA and MIGFA do not take advantage of polarimetric data at this time.

As for scan strategies, the introduction of the TDWR-inspired supplemental adaptive intra-volume low-level scan (SAILS) (Chrisman 2014) to WSR-88D in 2016 has given NWS radar operators options for volume coverage patterns (VCPs) that have more frequent surface scan updates, which is a key to timely microburst detections. SAILS is further subdivided into SAILxM, where  $M = 1, 2,$  or  $3$  corresponds to the number of additional base scan(s) inserted into the VCP. (The  $N > 1$  cases are referred to as MESO-SAILS, where MESO stands for “multiple elevation scan option.”) SAILS has proven to be popular (and effective) for hazardous weather warning decisions (Cho et al. 2022), which makes it more likely to be in effect for wind-shear cases. The automated volume scan evaluation and termination (AVSET; Chrisman 2013) algorithm also helps by shortening the volume update time whenever possible by adaptively skipping high-elevation-angle scans above  $5^\circ$  that contain no precipitation returns. After an initial trial period, AVSET has been on by default at all sites since 2012.

Due to the lingering uncertainties regarding WSR-88D wind-shear detection performance, and the fact that WSR-88D AMDA was not adapted to utilize the SAILS intra-volume surface scans until 2020, we decided to revisit the issue and conduct a large-volume analysis of WSR-88D AMDA performance. Microbursts were chosen first for study over gust fronts because they are more of a critical safety issue. Favorable results may lead to consideration of (1) in the short term, the possibility of adding operational microburst detection advisories at some airports with currently no service from the existing dedicated systems, and (2) in the long term, the potential for efficient tri-agency weather radar network consolidation in the U.S. (Weber et al. 2023).

## 2. METHODOLOGY

In order to assess microburst detection performance, the true state of the atmosphere must be known. As with most meteorological evaluation efforts, however, absolute truth is virtually impossible to obtain. In order to ascertain whether a microburst occurred or not (and to determine the outflow velocities accurately), one would need multiple sensor systems observing the area of interest at very fine spatial and temporal resolution, followed by human expert analysis of the aggregate data. In principle, this type of experiment is possible, but would be prohibitively expensive and time consuming to achieve statistically significant results.

The approach that we decided to take instead was to rely on the Integrated Terminal Weather System (ITWS; Evans and Ducot 1994) microburst detection product (Wolfson et al. 1994) as the “gold standard,” and compare the WSR-88D AMDA detections against that reference. The ITWS microburst detection algorithm underwent rigorous testing and validation prior to operational deployment, and utilizes TDWR data as well as local sounding data for background atmospheric stability information. (It also integrates LLWAS and lidar input where available.) With archived data going back to 2015 (albeit with varying levels of availability depending on time and location), there would be many cases available for reference. These data are not accessible by the public on the Internet, but may be obtained by request from the Department of Transportation’s Volpe National Transportation Systems Center.

As for the WSR-88D, we retrieved archived Level II data, which we then processed with an offline ORPG clone (Smalley et al. 2002) hosting AMDA. This procedure was necessary because WSR-88D AMDA products are not routinely archived, and also the AMDA version prior to 2020 was not able to ingest the intra-volume surface scans from SAILS. The WSR-88D Level II data are freely available via the National Oceanic and Atmospheric Administration (NOAA) National Center for Environmental Information (NCEI) data portal (<https://www.ncdc.noaa.gov/nexradinv/>) as well as from Google Cloud (<https://console.cloud.google.com/storage/browser/gcp-public-data-nexrad-12>). The detections generated by AMDA were then scored against the ITWS microburst detections. This evaluation scheme is illustrated in Figure 1.

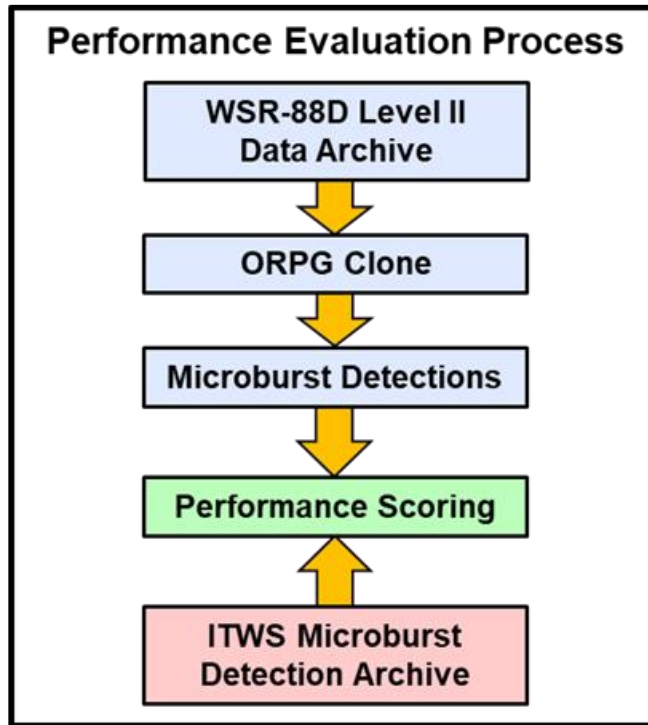


Figure 1. Framework for WSR-88D microburst detection performance assessment.

## 2.1 LOCATIONS

We selected 15 ITWS-serviced airports, where a nearby WSR-88D was projected to provide a decent level of microburst detection performance in the airport vicinity. These sites are listed in Table 1.

**TABLE 1**

**List of Airports Considered in Study**

Airport	Distance (km)	
	WSR-88D to Airport	WSR-88D to TDWR
Atlanta, GA (ATL)	33.3	42.2
Cleveland, OH (CLE)	0.9	18.4
Denver, CO (DEN)	13.8	6.8
Dulles, VA (IAD)	3.9	12.8
Indianapolis, IN (IND)	1.6	15.5
Houston/Hobby, TX (HOU)	27.3	16.5
Memphis, TN (MEM)	34.8	51.0

Miami, FL (MIA)	23.7	18.1
Nashville, TN (BNA)	17.1	31.0
Oklahoma City, OK (OKC)	21.5	22.0
Pittsburgh, PA (PIT)	4.6	22.9
St. Louis, MO (STL)	28.6	20.6
Tampa, FL (TPA)	32.6	20.6
Tulsa, OK (TUL)	29.2	26.3
Wichita, KS (ICT)	1.0	16.4

## 2.1 EVENT SEARCH PROCESS

We systematically searched for potential microburst events in the vicinity of the study airports in order to narrow the scope of the ITWS archived data requests. An automated script was written to filter NCEI storm events data (available at <https://www.ncdc.noaa.gov/stormevents/>) for thunderstorm wind, hail, lightning, and tornado events that occurred within a 20 km radius of the airports. We also captured events with any mention of microbursts in the event narrative within 50 km of the airport. We searched the years 2015–2022 to match ITWS data availability. Using MIT Lincoln Laboratory’s Corridor Integrated Weather System (CIWS) archival system, we manually played back precipitation intensity data in the airport vicinity around the event times to judge the time periods when microbursts may have occurred. We then submitted a request for archived ITWS data based on the list of time periods (and associated airports) found. Only some of the requested data were available, as the ITWS data archive do not have continuous coverage.

After receiving the ITWS data, we filtered them for microburst detections inside the nearby WSR-88D’s AMDA coverage range (60 km). The remaining data were used to determine the sites and time periods for procuring WSR-88D Level II data. A small fraction of cases was not available (likely due to the associated WSR-88D being down for maintenance or communication line disruptions). The resulting cases were then used in the study.

## 2.2 GEOMETRIC CONSIDERATIONS

Ideally, comparisons of weather observations between two radars should be made with both systems placed in the same location. Clearly, this is impossible for this study because all of the WSR-88Ds are separated from the TDWRs (Table 1). The azimuthal viewing angle is especially important for microbursts because the detection is made based on the line-of-sight (LOS) velocity shear only. This would not be an issue if microbursts were perfectly circular in the horizontal plane, but that is not the case; microbursts are often asymmetrical and present different radial shear values in different azimuthal directions (Hjelmfelt 1988; Hallowell 1993). We therefore decided to restrict the microburst detection comparisons to instances in which the LOS azimuthal viewing angle from the WSR-88D and the TDWR differed by no more than 25°. This was a compromise threshold reached by balancing the loss of usable data vs. comparison fidelity.

Performance scoring was also restricted to a region that was within 20 km from the airport reference point (ARP) and within the microburst detection product output ranges of ITWS (35 km from the TDWR) and WSR-88D AMDA (60 km from the WSR-88D).

With the enforcement of these geometric restrictions, we were left with 181 independent data periods from 14 WSR-88Ds (see Table 4 in Appendix A for a complete listing). All data cases from the Memphis (KNQA) WSR-88D were eliminated from further consideration.

### 2.3 DETECTIONS VS. EVENTS

The ITWS microburst output product, in part, consists of a circular polygon centered on the microburst and the peak velocity difference ( $\Delta V$ ) associated with the detection. The valid time period for the detection starts with the end time of the TDWR surface scan on which the  $\Delta V$  calculation was based and ends after the expiration time increment (120 s).

Because the TDWR surface scan updates every  $\sim 60$  s when weather is present, and ITWS refreshes its microburst detection with each of these updates, many ITWS microburst detection polygons overlap closely in space and time. In fact, they are often multiple detections of an ongoing microburst event. To obtain a more realistic and operationally relevant “truth” set, we grouped these cases into one merged space-time “event” given certain conditions. The procedure to do this was as follows. We operated on pairs of detections in chronological order, and if the valid time periods associated with the detection polygons overlapped and the criterion,

$$\frac{A_{Int}}{A_{Min}} \geq \frac{\Delta t_{Det}}{\tau_{Max}}, \quad (\text{Eq. 1})$$

was met, where  $A_{Int}$  is the intersection area between the polygons,  $A_{Min}$  is the area of the smaller polygon,  $\Delta t_{Det}$  is the difference in the detection times associated with the polygons (later minus earlier), and  $\tau_{Max}$  is the maximum reasonable lifetime of a microburst event, then the two detections were merged. The right-hand side of Equation 1 is capped at unity, and we set  $\tau_{Max} = 1800$  s after consulting Hjelmfelt (1988). The merged detection was assigned the larger of the two  $\Delta V$ s and the valid period was extended to the later expiration time. This process was repeated over all detections until no remaining detection pairs fulfilled the merging criteria. This process is illustrated visually in Figure 2.

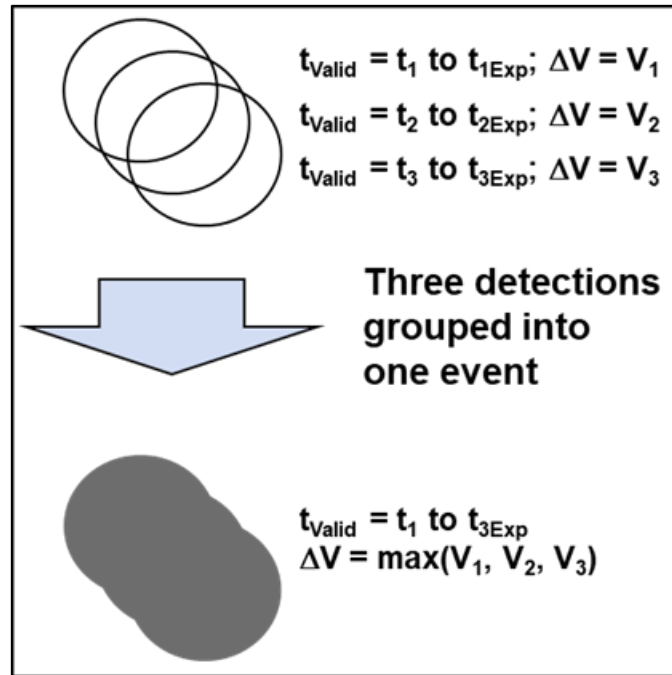


Figure 2. Illustration of the ITWS microburst detection merging process that results in an aggregate microburst event.

The concept behind Equation 1 is that the amount of spatial overlap between polygons (the left-hand side) indicates the degree of likelihood that the two detections are part of the same microburst event. However, if the detection times grow far apart (and this can happen after several polygons have been merged), then it becomes less likely that they are part of the same event. The time difference is normalized against a reasonable maximum lifetime for a microburst (the right-hand side). Consequently, the spatial overlap factor must outweigh the time separation factor for the detection merge to take place.

This polygon merging procedure was applied to the microburst detection output that was used as the reference event. For detection probability estimation, this reference was the ITWS microburst detection output. For false alarm probability estimation, this reference was the WSR-88D AMDA output. The next section explains how these estimates were made.

## 2.4 SCORING PROCEDURE

We adopted three performance metrics for this study: detection probability, false alarm probability, and median detection lag time. The raw detection probability was computed as the number of ITWS detections matched by WSR-88D detections divided by the number of ITWS detections. The raw false alarm probability was calculated as the number of WSR-88D detections not matched by ITWS detections divided by the number of WSR-88D detections. A detection match was declared if there was spatial and

temporal overlap between the ITWS microburst event and WSR-88D detection. The valid time periods for the event and detection were used in the overlap calculation. Since the WSR-88D AMDA detection output did not have a defined expiration time, we set it to 120 s to match the ITWS microburst product's expiration time. For both detection and false alarm probabilities, the “confirming” detection was allowed a 2.5-m s<sup>-1</sup> buffer below the minimum microburst alert value of 15 m s<sup>-1</sup> (30 kt) following the practice of past wind shear detection performance evaluations (Isaminger et al. 2000) to account for stochastic measurement errors. The median lag time was calculated as the median of the WSR-88D AMDA detection times minus the ITWS detection times.

However, because ITWS detections are not really the truth, i.e., they have detection probability less than one and false alarm probability greater than zero, the raw performance scores for WSR-88D AMDA as described above would be biased unfavorably. If we assume that missed detections by the two systems are statistically uncorrelated and false alarms by the two systems are also statistically uncorrelated, then we can derive normalization factors that would make the raw performance metrics more accurate. The raw WSR-88D microburst detection probability,  $P'_{dW}$ , is given by

$$P'_{dW} = \frac{N_{dW}P_{dI}}{NP_{dI}(1+P_{fI})}, \quad (\text{Eq. 2})$$

where  $N_{dW}$  is the true number of WSR-88D microburst detections,  $P_{dI}$  is the ITWS microburst detection probability,  $N$  is the true number of microburst events, and  $P_{fI}$  is the ITWS microburst false alarm probability. The numerator of Equation 2 shows the true number of WSR-88D detections reduced by the fact that the ITWS detection probability is less than one. The denominator of Equation 2 indicates that the true event count is reduced by the ITWS detection probability and inflated by the ITWS false alarm probability. The true WSR-88D microburst detection probability,  $P_{dW}$ , is defined by

$$P_{dW} = \frac{N_{dW}}{N}. \quad (\text{Eq. 3})$$

Combining Equations 2 and 3, then solving for  $P_{dW}$  yields

$$P_{dW} = P'_{dW}(1 + P_{fI}). \quad (\text{Eq. 4})$$

For the WSR-88D raw false alarm probability, we can rephrase its definition in complementary terms. In other words, one minus the raw WSR-88D false alarm probability,  $P'_{fW}$ , is equal to the number of WSR-88D detections matched by ITWS divided by the number WSR-88D detections. Since this quantity also describes the apparent ITWS detection probability,  $P'_{dI}$ , we can write

$$1 - P'_{fW} = P'_{dI}. \quad (\text{Eq. 5})$$

Using symmetry, we can then swap the “W” and “I” subscripts in Equations 2 and 3 to get

$$P'_{dI} = \frac{N_{dI}P_{dW}}{NP_{dW}(1+P_{fW})} \quad (\text{Eq. 6})$$

and

$$P_{dI} = \frac{N_{dI}}{N}. \quad (\text{Eq. 7})$$

Combining Equations 6 and 7, then solving for  $P_{fW}$  yields

$$P_{fW} = \frac{P_{dI}}{1 - P'_{fW}} - 1. \quad (\text{Eq. 8})$$

Knowledge of the true ITWS detection and false alarm probabilities are needed to compute Equations 4 and 8. Past studies have yielded  $P_{dI}$  in the range of 0.92 to 0.99, and  $P_{fI}$  in the range of 0 to 0.02 (Klinge-Wilson 1995; Dasey et al. 1996; Isaminger et al. 2000), depending on location, algorithm version, and evaluation method. As a reasonable average, we set  $P_{dI} = 0.96$  and  $P_{fI} = 0.01$ . Note that since  $P_{dI}$  is close to unity and  $P_{fI}$  is close to zero, the score normalization actually did not affect the end results too much.

Besides the detection and false alarm probabilities, we would also like to know the time difference statistics in detection. In other words, do the WSR-88D microburst detections lag behind ITWS? To characterize this quantity, we simply computed the time lag,  $T_{lag}$ , as the WSR-88D microburst detection time minus the ITWS microburst detection time. Both detection times are defined by the end times of the radar scans that were ingested by the detection algorithms.

An example of a confirmed microburst event detection around the Denver airport on 26 May 2019 is shown in Figure 3. At 22:25:00 UT, no microburst detection has been output. At 22:25:42 UT, ITWS first reports a detection (black polygon) with  $\Delta V = 20.6 \text{ m s}^{-1}$ . Note that this polygon shape is an aggregate of all detections (including from later times) as explained in Section 2.4. At 22:26:35 UT, the WSR-88D reports a microburst that overlaps in space and time with the ITWS detection, a confirmed event that is indicated by the polygons drawn in red. In this case,  $T_{lag}$  is 53s.

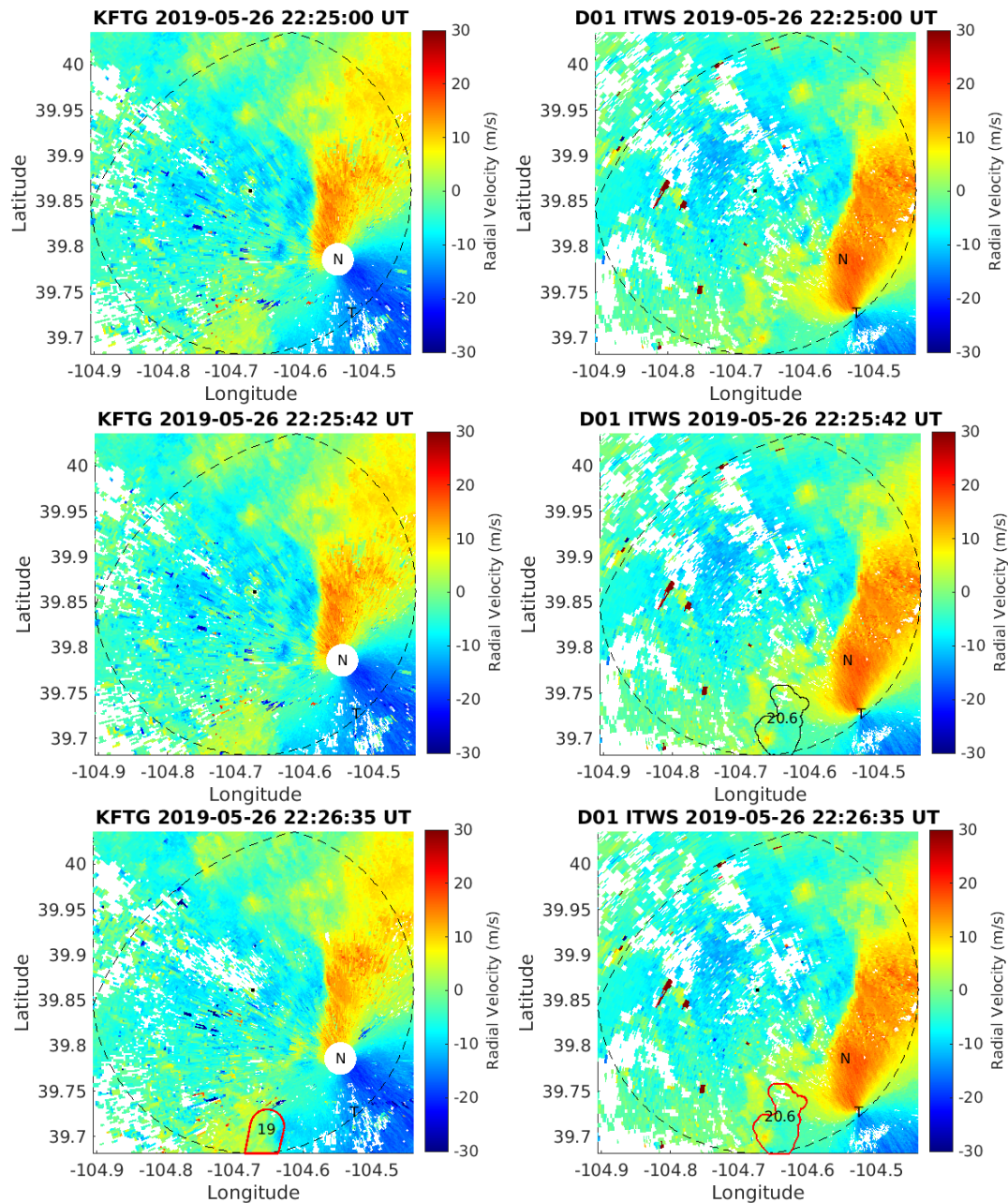


Figure 3. Microburst detection and lowest elevation angle radial velocity for WSR-88D (left) and ITWS (right) at Denver. White areas indicate invalid (censored) data. The airport reference point is denoted by the black dot in the center. The WSR-88D is located at the “N” and the TDWR is sited at the “T.” The scoring area (20 km from the airport and within microburst product output range of the WSR-88D and ITWS) is bounded by the black dashed line. The microburst  $\Delta V$  values ( $m s^{-1}$ ) are shown inside the microburst polygons. See main text for further details.

Even though Denver has the most favorable geometry for conducting a fair comparison between the WSR-88D and ITWS microburst detections due to the closeness (6.8 km) of the WSR-88D and TDWR, one can still see in Figure 3 that the radial velocity fields are certainly not the same, including the patterns of areas where data are marked as invalid. The antenna beamwidths are different ( $1^\circ$  for WSR-88D,  $0.5^\circ$  for TDWR), the lowest elevation angle is different ( $0.5^\circ$  for WSR-88D,  $0.3^\circ$  for TDWR), the operating band is different (S band for WSR-88D, C band for TDWR), the signal processing algorithms are different, the viewing geometry is different, and the data update times are different. All of these factors contribute to the differences observed in the radial velocity fields from the two radars. Furthermore, in addition to microbursts not necessarily being circularly symmetrical as explained in Section 2.3, velocity divergence phenomena other than microbursts that are not symmetrical at all (terrain-induced shear flows, gravity waves, etc.) can be interpreted to be microbursts by the detection algorithms. (One might say that these cases should be technically categorized as false detections since they are not microbursts, but, operationally, any strong velocity divergence is an aviation hazard, so we would argue that they should be considered valid detections.) These considerations make a 100% fair comparison of WSR-88D and ITWS microburst detections nearly impossible. By compiling a big set of cases for the performance evaluation, we are relying on the statistics of large numbers to average out spurious results.

A time-lapse video of another example case was presented at the 23rd Conference on Aviation, Range, and Aerospace Meteorology, presentation number 2.1. The recording of this presentation is available online at <https://ams.confex.com/ams/103ANNUAL/meetingapp.cgi/Session/62343>. The case example is shown starting at the 7:07 mark of the recording.

**This page intentionally left blank.**

### 3. RESULTS

Examining the initial results, it became clear that distance between the WSR-88D and the microburst had a big impact on the detection performance. This was not surprising, since microburst outflows occur close to the ground and the radar's minimum observable height increases with range. Therefore, we have parsed the detection performance statistics using this variable. Table 2 shows the results.

**TABLE 2**  
**WSR-88D AMDA Performance**

WSR-88D range to event (km)	$P_d$ (%)	$N$ for $P_d$	$P_f$ (%)	$N$ for $P_f$	$T_{lag}$ (s)	$N$ for $T_{lag}$
0–10	93.2 <b>86.6</b> 75.3	56	12.4 <b>7.2</b> 4.1	153	46 <b>3</b> -22	48
0–20	96.9 <b>94.8</b> 91.2	244	7.5 <b>5.4</b> 3.9	614	46 <b>36</b> 16	229
0–30	93.1 <b>90.5</b> 87.0	355	7.0 <b>5.2</b> 3.9	786	42 <b>26</b> 12	318
0–40	83.5 <b>80.2</b> 76.4	490	8.8 <b>7.0</b> 5.5	905	42 <b>29</b> 12	389
0–50	77.7 <b>74.4</b> 70.8	607	9.8 <b>8.0</b> 6.4	975	46 <b>36</b> 22	447
0–60	77.2 <b>73.9</b> 70.3	611	9.8 <b>8.0</b> 6.4	975	46 <b>36</b> 22	447
10–20	98.8 <b>97.2</b> 93.8	188	7.2 <b>4.9</b> 3.3	461	51 <b>41</b> 21	181
20–30	87.2 <b>81.0</b> 72.7	111	8.7 <b>4.5</b> 2.3	172	42 <b>7</b> -2	89
30–40	61.3 <b>53.1</b> 44.7	135	28.4 <b>20.3</b> 14.0	119	69 <b>31</b> -1	71
40–50	59.0 <b>50.1</b> 41.2	117	33.2 <b>22.2</b> 14.0	70	170 <b>103</b> 49	58

In Table 2, the  $P_d$  and  $P_f$  values are shown (bold) in the center of the cells along with the upper and lower limits of the 95% confidence interval based on the Wilson (1927) score method. We chose this formulation due to its conservativeness (on average), coverage probability being consistent and close to the nominal level, and relatively good accuracy even for small sample sizes (Pobocikova 2010). For  $T_{lag}$ , the median is shown (bold) along with the upper and lower limits of the 95% confidence interval following a rank-ordering technique (Conover 1999). The number of data points used ( $N$ ) to calculate these quantities is also shown.

For reference, the Federal Aviation Administration’s (FAA) requirements for wind shear detection  $P_d$  and  $P_f$  are listed in Table 3. As the definition of microburst is  $\Delta V \geq 30$  kt, and that is the threshold used in this study, we can compare the results of Table 2 to the  $\Delta V \geq 30$  kt detection requirements in Table 3 (emphasized in bold). It is clear that once the WSR-88D is farther than  $\sim 30$  km from a microburst event, the detection performance falls steeply below the minimum operationally acceptable levels as implied by the WSP requirements. Although there is uncertainty in the results as characterized by the 95% confidence intervals, it appears that a WSR-88D that is 20–30 km from a microburst would provide a WSP level of performance, whereas a WSR-88D that is up to 20 km from a microburst would provide an ITWS level of performance, despite the fact that it does not have access to auxiliary data ingested by ITWS nor employs the more advanced algorithms implemented in ITWS. A caveat to this last statement is that WSR-88D’s performance appears to be worse at the closest ranges (0–10 km) compared to the 10–20 km bin. This is most likely due to the WSR-88D not outputting valid velocity data in the 0–2 km range. This lack of near-range data is evident in the white disk around the “N” in Figure 3. This lack of the first eight range gates is common to all WSR-88Ds, and is the result of those gates being generally deemed unreliable, likely due to receiver saturation from nearby ground clutter. The WSR-88D is therefore not quite meeting the system minimum base velocity output range of 1 km (Section 3.7.2.2.1.1.2 in ROC (2008)). The TDWR avoids this problem by employing a front-end sensitivity time control (STC) mechanism (Michelson et al. 1990) and a very high dynamic range receiver (Cho et al. 2005). The radar functional requirements (RFR) document (NOAA 2015) that is aimed at whatever system replaces the WSR-88D in the future does not include a minimum observation range requirement. We recommend that such a requirement be added with a value comparable to the TDWR’s 0.25 nautical mile (NM) (0.5 km) (FAA 1995).

**TABLE 3**

**Wind Shear Detection Performance Requirements**

System	$\Delta V$			
	$\geq 15$ kt	$\geq 20$ kt	$\geq 30$ kt	$\geq 40$ kt
ITWS (FAA 1995)	$P_d \geq 90\%$ $P_f \leq 5\%$	—	<b><math>P_d \geq 95\%</math></b> <b><math>P_f \leq 5\%</math></b>	—
TDWR (FAA 1987)	—	$P_d \geq 90\%$ $P_f \leq 10\%$	—	—
ASR-9 WSP (FAA 2009)	—	$P_d \geq 70\%$ $P_f \leq 20\%$	<b><math>P_d \geq 80\%</math></b> <b><math>P_f \leq 15\%</math></b>	$P_d \geq 90\%$ $P_f \leq 10\%$

Regarding how far a WSR-88D can be from the ARP to provide these projected levels of microburst detection performance, we need to take into account that microburst alerts are reported only within the area noted for attention (ARENA), which is defined by 1-NM-wide squares centered on the airport runways and the lines along the approach and departure corridors extended for 3 NM beyond the runway ends. Conservatively assuming that the longest half-length of a runway is no more than 1.3 NM (e.g., runway 16R/34L at Denver, the longest runway in the U.S.), then the distance past the ARP that must be covered for microburst alerts by the WSR-88D would be 4.3 NM or 8 km. Putting this together with the results from Table 2, we project (for coverage over the ARENA) ITWS-level  $P_d$  and  $P_f$  for WSR-88D up to ~12 km from the ARP and at least WSP-level  $P_d$  and  $P_f$  up to ~22 km from the ARP. For comparison, TDWRs are located 10 to 24 km from ARPs, and during deployment planning it was thought that 14–22 km from the ARP would generally provide the best viewing angles over the airport, considering factors like ground clutter and the radar’s cone of silence (Evans and Bernella 1994).

As for  $T_{lag}$ , there does not seem to be a clear dependence on distance between radar and event, except perhaps at the extreme far range (40–50 km) where  $T_{lag}$  is significantly longer. Though the ITWS microburst product output is updated every 60 s (matching the 60-s update period of the TDWR’s base (lowest elevation) scans in hazardous volume scanning mode), the WSR-88D AMDA output rate depends on the base scan update interval, which varies with the VCP mode selected by the NWS WFO radar operator. We hypothesized that  $T_{lag}$  may be impacted by the WSR-88D’s base scan update period at the time of the microburst detection. In order to investigate this proposition, we obtained WSR-88D archive III status product (ASP) data, which contain per-volume-scan information on time, VCP number, VCP option status, and volume scan duration. ASP data are available from NCEI (<https://www.ncdc.noaa.gov/nexradinv/>) as well as from Google Cloud (<https://console.cloud.google.com/storage/browser/gcp-public-data-nexrad-13/2019/12?authuser=0&prefix>).

Figure 4 shows the histogram of WSR-88D base scan update period at the times of detection, missed detection, and false alarm for the WSR-88D to event range 0–30 km category. (This category was chosen, because it is most relevant for application to an operational scenario.) There are four distinct modes in the distribution corresponding to the SAILSx3 (~95 s), SAILSx2 (~115 s), SAILSx1 (~160 s), and SAILS off (~275 s) VCP options. The spread within each mode is due to the volume scan update interval dependence on the root VCP choice and the real-time variance introduced by AVSET.

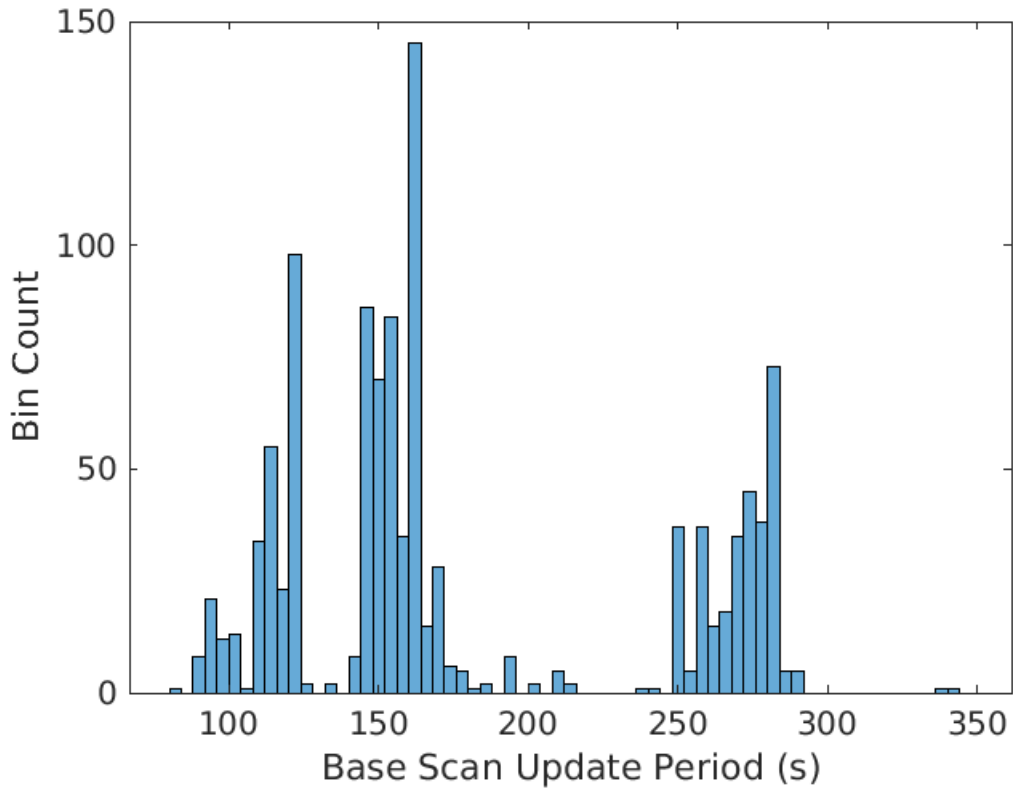


Figure 4. Histogram of WSR-88D base scan update period at the times of microburst detection, missed detection, and false alarm for the 0–30-km radar-to-event range category.

Figure 5 shows the histogram of  $T_{lag}$  for the 0–30-km WSR-88D-to-event range category. Note that the mode of the distribution is at 0 s, and most of data fall into a fairly symmetric pseudo-Gaussian shape from  $\sim -100$  s to  $\sim 100$  s. This means that the positive median  $T_{lag}$  of 26 s (Table 2) resulted from the long thin tail in the distribution above  $\sim 150$  s. If the tail could be eliminated, then there would effectively be no lag time on average for WSR-88D microburst detections compared to ITWS microburst detections.

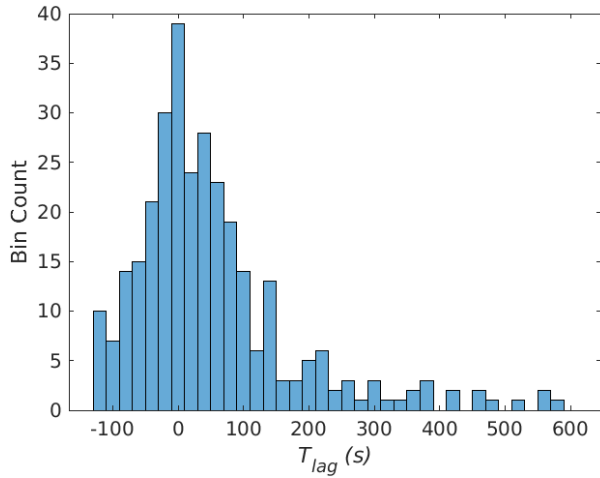


Figure 5. Histogram of  $T_{lag}$  for the 0–30-km WSR-88D-to-event range category.

Figure 6 shows the histogram of  $T_{lag}$  for the 0–30-km WSR-88D-to-event range category and radar base scan update period less than or equal to 120 s. Relative to Figure 5, much of the thin long tail in the distribution has been filtered out, with the resulting median  $T_{lag}$  reduced to 12 s (with lower and upper 95% confidence limits of -5 s and 20 s).

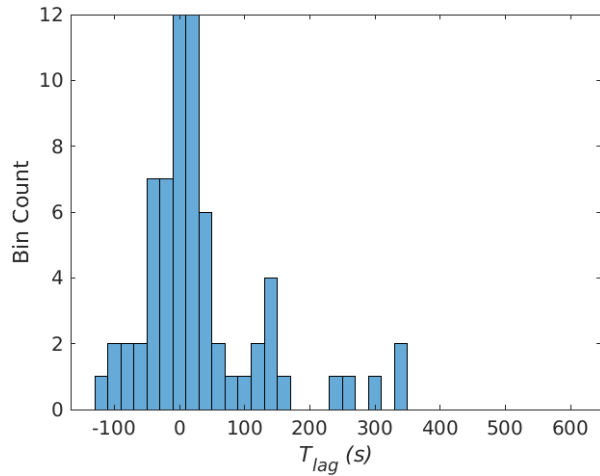


Figure 6. Histogram of  $T_{lag}$  for the 0–30-km WSR-88D-to-event range category and WSR-88D base scan update period less than or equal to 120 s.

Figure 7 shows the histogram of  $T_{lag}$  for the 0–30-km WSR-88D-to-event range category and radar base scan update period greater than or equal to 240 s. Compared to Figure 5, the tail-to-mode ratio in the distribution is higher, with the resulting median  $T_{lag}$  increased to 40 s (with lower and upper 95% confidence limits of 23 s and 72 s). Thus, when the WSR-88D was operated in the MESO-SAILS modes (SAILSx2 and SAILSx3), the median  $T_{lag}$  was significantly (at greater than 95% confidence level) shorter than when the radar was operated in SAILS-off mode. These results confirm our hypothesis that  $T_{lag}$  was impacted by the WSR-88D’s base scan update period at the time of the microburst detection.

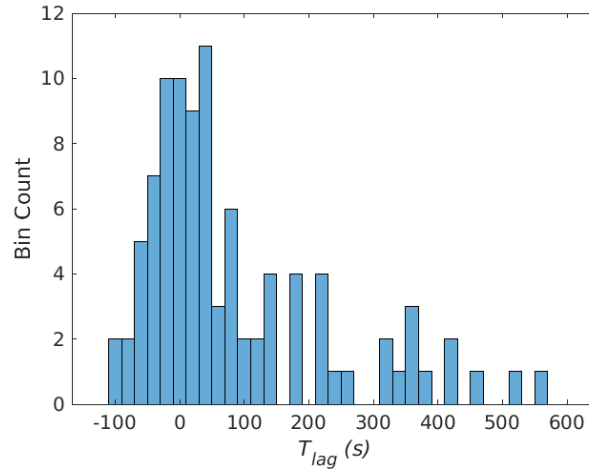


Figure 7. Histogram of  $T_{lag}$  for the 0–30-km WSR-88D-to-event range category and WSR-88D base scan update period greater than or equal to 240 s.

One wrinkle that should be mentioned is that several WSR-88Ds have implemented elevation angle scans that are lower than the standard angle of  $0.5^\circ$  in order to improve low-altitude coverage where the radar is located significantly higher than the surrounding terrain. ORPG AMDA does not utilize these scans, in part, due to concerns about data quality (e.g., ground clutter residue). However, because the SAILS base scans correspond to these lowest angle scans instead of the  $0.5^\circ$  scans at these sites, AMDA cannot take advantage of those more rapidly updated SAILS scans. Of the WSR-88Ds in this study, only Cleveland (KCLE) has these “extra low” elevation scans, and since it was not implemented until 22 October 2020, only the 23 October 2020 (Table 4) data were affected.

Another minor point to note is that there were a small number of instances in which the mid-volume rescan of low-level elevations (MRLE; Chrisman 2016) VCP option was used. MRLE is similar to SAILSx1, except other low-level elevations scans (e.g.,  $0.9^\circ$ ,  $1.3^\circ$ , and  $1.8^\circ$ ) are updated more frequently as well. Since the national rollout of MRLE began in May 2018 to the end of 2020, MRLE has been used on just 0.14% of volume scans, including only the post-deployment period at each site (Cho et al. 2022).

MRLE's impact on base scan update period and AMDA performance is expected to be similar to that of SAILSx1.

**This page intentionally left blank.**

## 4. SUMMARY DISCUSSION

We evaluated WSR-88D AMDA microburst detection performance using TDWR-based ITWS microburst detections as reference. In order to conduct a fair comparison between the two systems, we restricted the event pool to those that had azimuthal viewing angles from the radars that differed by no more than  $25^\circ$ . This resulted in 181 independent data time periods from 14 airport areas, spanning 2015–2022. We also grouped individual reference detections into aggregated events that better reflected the microburst phenomenology. Finally, we formulated score normalization equations to account for the imperfect nature of the reference system (ITWS) performance.

Our study showed that the detection and false alarm probabilities depended on event range from the radar. ITWS-like  $P_d$  and  $P_f$  ( $\sim 95\%$  and  $\sim 5\%$ ) were achieved for 0 to 20 km range, whereas at 20 to 30 km,  $P_d$  and  $P_f$  ( $\sim 80\%$  and  $\sim 5\%$ ) meeting or exceeding WSP requirements ( $P_d \geq 80\%$  and  $P_f \leq 15\%$ ) were seen. Beyond about 30 km from the radar, the microburst detection performance fell to unacceptable levels. Conservatively adding a margin of 8 km to account for the need to cover the entire ARENA extending on the other side of the airport, we project (for coverage over the ARENA) ITWS-level  $P_d$  and  $P_f$  for WSR-88D up to  $\sim 12$  km from the ARP and at least WSP-level  $P_d$  and  $P_f$  up to  $\sim 22$  km from the ARP.

Analysis of the detection timing indicated that, on average, WSR-88D AMDA lagged ITWS, with a median value on the order of 30 s. Taken at face value, this level of lag time may be acceptable, given that it is only about half of the ITWS microburst detection update requirement of 60 s. However, examination of the lag distribution showed a thin positive tail extending out to  $\sim 600$  s. That level of detection lag, albeit for a small minority of cases, should be eliminated for operational ATC usage. We showed that the lag distribution tail can be shortened if the WSR-88D's slowest base scan update modes are eliminated. This brings up a crucial point—because the WSR-88D's VCP mode is controlled manually by NWS WFO forecasters, the radar can be put into a mode that may be optimized for observation of phenomena other than microbursts and gust fronts. For example, a meteorologist wanting to monitor the vertical structure of a rapidly growing storm cell may wish to emphasize more frequent volume scan updates at the expense of sparser base scan updates. There are a couple of approaches to addressing this issue.

- In the relatively short term, with recent studies showing that faster base scan updates lead to improved severe weather warning performance, even at the expense of slower volume scan updates in many cases (Cho et al. 2022), one could consider imposing a maximum base scan update period on all WSR-88D non-clear-air VCPs at sites where the radar would be used to provide airport wind-shear detection services. This would likely mean that all non-clear-air VCPs used at these sites would have scanning patterns that are MESO-SAILS-like and/or with upper elevation angles that are more sparsely sampled like the TDWR hazard scans. Such a measure would need to be developed and approved by the tri-agency Radar Operations Center (ROC) in consultation with the WFOs. There may also need to be a “fail safe” feature added at these sites that would automatically override the selection of a clear-air VCP when any significant weather

is detected in the airport vicinity, analogous to how the TDWR automatically switches from monitor to hazard scan mode in the presence of weather.

- For the long term, the requirements for the WSR-88D follow-on radar call for a “threshold” update period of 90 s for low-altitude severe weather surveillance and an “objective” volume scan update period of 60 s (NOAA 2022). A future radar that met the latter requirement level would certainly be capable of providing operationally acceptable wind-shear detection update times. Even only meeting the former requirement level may be enough, although if there are still scan mode options that are allowed to have low-altitude update periods greater than 90 s, measures discussed in the bullet above may still be needed.

Another point of concern for the WSR-88D is the lack of output data from the first eight range gates (2 km). This near-range blind zone creates a hole in the data that, for sites that are very close to the airport, can lead to missed microburst detections in the ARENA. To eliminate this problem for the future WSR-88D replacement, we recommend that a minimum observation range requirement comparable to the TDWR’s (0.5 km) be added to the follow-on radar program requirements.

Finally, there are qualifiers to this study that should be reiterated. The ITWS microburst detections are merely a proxy for truth; absolute truth is not available, especially for past events. Although we have gone to great lengths to compensate for this shortfall, there is some inevitable degree of uncertainty in the results. On the positive side, there is potential for even better WSR-88D microburst detection performance if the algorithm is enhanced to include sounding and model data that ITWS uses, as well as the polarimetric variables that have not been exploited in the past. For example, specific differential phase core characteristics, which have some predictive powers for downburst occurrence (Kuster et al. 2021), may help enable earlier declarations of microburst detections. This is an activity that we recommend take place in the future.

## APPENDIX A DATA LIST

**TABLE 4**

**WSR-88D Data Periods Used in Study**

<b>Site</b>	<b>Start Time (UT)</b>	<b>End Time (UT)</b>
KAMX	6/29/2015 18:45	6/29/2015 21:35
KAMX	8/9/2016 21:00	8/9/2016 23:55
KAMX	8/25/2018 14:35	8/25/2018 16:55
KAMX	5/18/2020 20:45	5/19/2020 0:40
KAMX	5/29/2022 18:25	5/29/2022 21:35
KAMX	6/9/2022 16:35	6/9/2022 19:45
KAMX	7/26/2022 16:05	7/26/2022 17:45
KCLE	8/10/2016 0:50	8/10/2016 2:00
KCLE	8/11/2016 20:00	8/11/2016 21:30
KCLE	4/19/2017 20:30	4/19/2017 22:50
KCLE	7/5/2018 19:00	7/5/2018 21:10
KCLE	9/5/2018 21:50	9/5/2018 23:10
KCLE	6/28/2019 22:00	6/28/2019 23:50
KCLE	8/6/2019 15:45	8/6/2019 20:00
KCLE	9/13/2019 23:20	9/14/2019 2:00
KCLE	10/23/2020 21:50	10/23/2020 23:30
KFFC	6/15/2017 21:15	6/15/2017 23:15
KFFC	7/21/2018 22:30	7/21/2018 23:45
KFFC	7/9/2021 17:00	7/9/2021 20:10
KFTG	6/24/2015 22:45	6/25/2015 0:50
KFTG	7/21/2015 19:45	7/21/2015 21:30
KFTG	7/24/2016 21:50	7/24/2016 23:50
KFTG	7/4/2017 21:50	7/4/2017 23:20
KFTG	8/5/2017 1:00	8/5/2017 3:20
KFTG	7/3/2018 3:50	7/3/2018 6:10
KFTG	7/23/2018 22:00	7/24/2018 0:30
KFTG	7/27/2018 2:45	7/27/2018 4:00
KFTG	5/26/2019 21:50	5/26/2019 23:59
KFTG	5/27/2019 22:20	5/27/2019 23:30
KFTG	7/22/2019 22:40	7/22/2019 23:59
KFTG	7/30/2019 22:30	7/31/2019 2:10

KFTG	6/6/2020 21:40	6/6/2020 23:20
KFTG	7/10/2020 2:40	7/10/2020 4:10
KFTG	7/4/2021 20:30	7/4/2021 23:59
KFTG	7/5/2021 23:15	7/6/2021 0:30
KHGX	8/11/2015 22:20	8/12/2015 0:10
KHGX	5/21/2016 21:05	5/21/2016 23:10
KHGX	8/27/2017 1:30	8/27/2017 5:10
KHGX	4/4/2018 4:25	4/4/2018 5:30
KHGX	5/27/2018 1:35	5/27/2018 4:10
KHGX	7/31/2018 16:40	7/31/2018 18:00
KHGX	4/7/2019 17:10	4/7/2019 18:10
KHGX	8/28/2019 22:00	8/28/2019 23:15
KHGX	5/27/2020 20:55	5/27/2020 22:25
KHGX	6/15/2021 22:00	6/16/2021 1:30
KHGX	12/18/2021 17:30	12/18/2021 19:30
KICT	6/16/2017 0:00	6/16/2017 2:15
KICT	9/25/2017 18:00	9/25/2017 20:50
KICT	6/27/2018 0:30	6/27/2018 4:20
KICT	5/24/2019 21:30	5/24/2019 23:05
KICT	6/22/2019 23:00	6/23/2019 2:15
KICT	8/22/2019 0:25	8/22/2019 7:20
KICT	7/30/2020 1:10	7/30/2020 4:00
KICT	3/12/2021 11:50	3/12/2021 12:45
KICT	7/26/2021 19:30	7/26/2021 22:30
KIND	7/14/2015 0:50	7/14/2015 6:45
KIND	7/17/2015 18:40	7/17/2015 23:50
KIND	5/2/2016 0:50	5/2/2016 2:25
KIND	5/12/2016 0:00	5/12/2016 1:20
KIND	6/15/2016 19:55	6/15/2016 23:05
KIND	7/13/2016 20:20	7/13/2016 23:25
KIND	6/13/2017 15:10	6/13/2017 17:45
KIND	7/7/2017 19:45	7/7/2017 23:15
KIND	5/16/2019 21:10	5/16/2019 22:20
KIND	5/23/2020 17:15	5/23/2020 19:00
KIND	8/25/2021 14:30	8/25/2021 18:00
KINX	4/26/2017 3:00	4/26/2017 4:50
KINX	5/11/2017 18:30	5/11/2017 23:50
KINX	5/19/2017 1:00	5/19/2017 4:10

KINX	5/20/2017 0:00	5/20/2017 1:00
KINX	8/6/2017 6:00	8/6/2017 7:00
KINX	8/7/2018 20:40	8/7/2018 23:10
KINX	8/16/2018 19:15	8/16/2018 23:59
KINX	5/21/2019 0:00	5/21/2019 4:00
KINX	6/23/2019 11:20	6/23/2019 13:50
KINX	7/22/2019 4:45	7/22/2019 6:00
KINX	4/24/2020 22:10	4/24/2020 23:20
KINX	7/12/2020 1:30	7/12/2020 4:00
KINX	11/11/2021 0:50	11/11/2021 2:00
KINX	12/6/2021 1:50	12/6/2021 3:45
KLSX	4/29/2017 20:10	4/29/2017 21:30
KLSX	5/29/2017 21:00	5/29/2017 23:00
KLSX	6/14/2017 16:40	6/14/2017 17:45
KLSX	6/18/2017 5:50	6/18/2017 7:00
KLSX	7/23/2017 7:20	7/23/2017 10:10
KLSX	6/9/2018 14:45	6/9/2018 17:50
KLSX	6/28/2018 22:00	6/29/2018 0:10
KLSX	5/21/2019 23:25	5/22/2019 0:30
KLSX	5/29/2019 22:10	5/29/2019 23:55
KLSX	6/2/2019 0:15	6/2/2019 4:00
KLSX	6/26/2019 19:35	6/26/2019 21:25
KLSX	7/15/2020 19:50	7/15/2020 22:05
KLSX	7/19/2020 23:40	7/20/2020 2:15
KLSX	6/19/2021 20:45	6/19/2021 23:20
KLSX	7/10/2021 1:25	7/10/2021 6:30
KLSX	8/8/2021 20:40	8/8/2021 22:15
KLSX	8/23/2021 19:30	8/23/2021 22:10
KLSX	8/26/2021 18:15	8/26/2021 21:40
KLSX	9/14/2021 21:20	9/14/2021 23:35
KLWX	6/18/2015 19:20	6/18/2015 21:30
KLWX	6/20/2015 23:15	6/21/2015 0:15
KLWX	6/23/2015 22:15	6/23/2015 23:45
KLWX	8/4/2015 21:00	8/4/2015 23:59
KLWX	6/16/2016 22:30	6/17/2016 1:40
KLWX	6/21/2016 17:10	6/21/2016 23:15
KLWX	9/7/2016 22:00	9/7/2016 22:50
KLWX	5/18/2017 22:50	5/19/2017 0:40

KLWX	5/31/2017 20:50	5/31/2017 21:50
KLWX	7/7/2017 23:15	7/8/2017 0:15
KLWX	7/14/2017 19:30	7/14/2017 21:00
KLWX	8/3/2017 20:45	8/4/2017 0:40
KLWX	5/23/2019 18:55	5/23/2019 19:55
KLWX	5/30/2019 18:35	5/30/2019 20:00
KLWX	6/27/2019 20:30	6/27/2019 23:30
KLWX	7/2/2019 20:00	7/2/2019 23:59
KLWX	7/17/2019 20:35	7/17/2019 21:50
KLWX	8/7/2019 17:20	8/7/2019 20:20
KLWX	8/15/2019 18:20	8/15/2019 20:10
KLWX	8/17/2019 22:50	8/18/2019 0:20
KLWX	8/20/2019 0:15	8/20/2019 3:20
KLWX	8/20/2019 20:00	8/20/2019 23:30
KLWX	9/2/2019 20:40	9/2/2019 23:40
KLWX	6/4/2020 22:50	6/5/2020 0:20
KLWX	6/22/2020 19:00	6/22/2020 22:30
KLWX	7/20/2020 19:45	7/20/2020 22:40
KLWX	7/22/2020 18:40	7/22/2020 19:45
KLWX	5/4/2021 20:00	5/4/2021 21:30
KLWX	7/26/2021 22:15	7/26/2021 23:45
KLWX	8/10/2021 20:00	8/10/2021 22:30
KLWX	8/27/2021 18:15	8/27/2021 20:00
KLWX	9/1/2021 6:00	9/1/2021 7:30
KOHX	3/1/2017 12:45	3/1/2017 13:45
KPBZ	6/19/2015 0:00	6/19/2015 1:20
KPBZ	8/22/2017 17:00	8/22/2017 20:10
KPBZ	6/13/2018 22:30	6/14/2018 0:50
KPBZ	6/22/2022 20:00	6/22/2022 22:25
KTBW	4/6/2017 8:40	4/6/2017 10:15
KTBW	6/7/2017 12:30	6/7/2017 14:10
KTBW	6/11/2017 18:40	6/11/2017 21:15
KTBW	6/14/2017 19:45	6/14/2017 20:55
KTBW	6/22/2017 23:20	6/23/2017 1:55
KTBW	7/5/2017 22:10	7/6/2017 1:00
KTBW	7/10/2017 20:05	7/10/2017 22:45
KTBW	5/24/2018 22:15	5/24/2018 23:50
KTBW	7/23/2018 8:00	7/23/2018 9:10

KTBW	8/25/2018 18:45	8/25/2018 22:20
KTBW	8/28/2018 20:10	8/28/2018 21:50
KTBW	8/29/2018 19:10	8/29/2018 20:50
KTBW	9/21/2018 18:00	9/21/2018 19:45
KTBW	11/2/2018 18:45	11/2/2018 19:45
KTBW	4/19/2019 16:50	4/19/2019 18:20
KTBW	4/30/2019 21:00	4/30/2019 22:40
KTBW	6/28/2019 20:05	6/28/2019 22:20
KTBW	7/4/2019 17:25	7/4/2019 19:20
KTBW	7/20/2019 0:00	7/20/2019 1:35
KTBW	7/20/2019 19:30	7/20/2019 23:05
KTBW	7/31/2019 21:45	7/31/2019 23:40
KTBW	9/18/2019 21:30	9/18/2019 23:45
KTBW	4/20/2020 15:30	4/20/2020 17:20
KTBW	4/24/2020 9:30	4/24/2020 10:50
KTBW	6/14/2020 22:00	6/15/2020 1:50
KTBW	7/18/2020 17:45	7/18/2020 20:30
KTBW	8/9/2020 3:20	8/9/2020 4:50
KTBW	9/6/2020 21:20	9/6/2020 23:10
KTBW	9/7/2020 18:45	9/7/2020 21:45
KTBW	6/29/2021 19:00	6/29/2021 21:50
KTBW	7/12/2021 18:10	7/12/2021 20:15
KTLX	4/21/2017 11:20	4/21/2017 15:00
KTLX	4/29/2017 9:40	4/29/2017 11:45
KTLX	5/17/2017 5:30	5/17/2017 6:40
KTLX	7/15/2017 20:00	7/15/2017 23:15
KTLX	10/22/2017 0:30	10/22/2017 2:10
KTLX	5/18/2019 12:00	5/18/2019 14:10
KTLX	5/26/2019 3:15	5/26/2019 6:00
KTLX	8/27/2019 2:00	8/27/2019 5:45
KTLX	6/21/2020 11:10	6/21/2020 12:40
KTLX	7/12/2020 4:20	7/12/2020 5:40
KTLX	4/29/2021 1:30	4/29/2021 2:15
KTLX	7/26/2021 19:30	7/26/2021 21:30
KTLX	8/16/2021 23:00	8/17/2021 2:00
KTLX	10/15/2021 4:30	10/15/2021 6:15

**This page intentionally left blank.**

## **ACKNOWLEDGMENTS**

We would like to thank Shane Kent (Volpe National Transportation Systems Center) for retrieving, parsing, and packaging the requested ITWS archive data, and our MIT Lincoln Laboratory colleagues Dave Smalley, Mark Veillette, and Mike Donovan for sundry assistance.

**This page intentionally left blank.**

## GLOSSARY

AMDA	Automated Microburst Detection Algorithm
ARENA	Area Noted for Attention
ARP	Airport Reference Point
ASP	Archive III Status Product
ASR-9	Airport Surveillance Radar-9
ATC	Air Traffic Control
AVSET	Automated Volume Scan Evaluation and Termination
CIWS	Corridor Integrated Weather System
FAA	Federal Aviation Administration
ITWS	Integrated Terminal Weather System
LLWAS	Low-Level Wind Shear Alert System
LOS	Line of Sight
MESO	Multiple Elevation Scan Option
MIGFA	Machine Intelligent Gust Front Algorithm
MRLE	Mid-Volume Rescan of Low-Level Elevations
NCEI	National Center for Environmental Information
NEXRAD	Next-Generation Weather Radar
NOAA	National Oceanic and Atmospheric Administration
NWS	National Weather Service
ORPG	Open Radar Product Generator
RF	Radio Frequency
RFR	Radar Functional Requirements
ROC	Radar Operations Center
SAILS	Supplemental Adaptive Intra-Volume Low-Level Scan
SCR	Signal-to-Clutter Ratio
STC	Sensitivity Time Control
TDWR	Terminal Doppler Weather Radar
UT	Universal Time
VCP	Volume Coverage Pattern
WFO	Weather Forecast Office
WSP	Weather Systems Processor
WSR-88D	Weather Surveillance Radar 1988-Doppler

**This page intentionally left blank.**

## REFERENCES

- [1.] Cho, J. Y. N., 2015: Enhanced signal processing algorithms for the ASR-9 Weather Systems Processor. *J. Atmos. Oceanic Technol.*, **32**, 1847–1859, <https://doi.org/10.1175/JTECH-D-15-0003.1>.
- [2.] Cho, J. Y. N., and R. G. Hollowell, 2008: Detection probability modeling for airport wind-shear sensors. Project Rep. ATC-340, MIT Lincoln Laboratory, Lexington, MA, 73 pp., [https://www.ll.mit.edu/sites/default/files/publication/doc/2019-01/Cho\\_2008\\_ATC-340\\_WW-18718.pdf](https://www.ll.mit.edu/sites/default/files/publication/doc/2019-01/Cho_2008_ATC-340_WW-18718.pdf).
- [3.] Cho, J. Y. N., and M. E. Weber, 2010: Terminal Doppler Weather Radar enhancements. *Proc. 2010 IEEE Radar Conf.*, 1245–1249, <https://doi.org/10.1109/RADAR.2010.5494427>.
- [4.] Cho, J. Y. N., G. R. Elkin, and N. G. Parker, 2005: Enhanced radar data acquisition system and signal processing algorithms for the Terminal Doppler Weather Radar. In *32<sup>nd</sup> Conf. on Radar Meteorology*, Albuquerque, NM, Amer. Meteor. Soc., P4R.8, <http://ams.confex.com/ams/pdfpapers/96018.pdf>.
- [5.] Cho, J. Y. N., R. S. Frankel, M. F. Donovan, M. S. Veillette, and P. L. Heinselman, 2013: Wind-shear detection performance study for MPAR risk reduction. In *36<sup>th</sup> Conf. on Radar Meteorology*, Breckenridge, CO, Amer. Meteor. Soc., 3B.3, [https://ams.confex.com/ams/36Radar/webprogram/Manuscript/Paper228623/Cho\\_3B3.pdf](https://ams.confex.com/ams/36Radar/webprogram/Manuscript/Paper228623/Cho_3B3.pdf).
- [6.] Cho, J. Y. N., and co-authors, 2022: Impact of WSR-88D intra-volume low-level scans on severe weather warning performance. *Wea. Forecasting*, **37**, 1169–1189, <https://doi.org/10.1175/WAF-D-21-0152.1>.
- [7.] Chrisman, J. N., 2013: Dynamic scanning. *NEXRAD Now*, **22**, NOAA/NWS/Radar Operations Center, Norman, OK, 1–3, <https://www.roc.noaa.gov/WSR88D/PublicDocs/NNOW/NNow22c.pdf>.
- [8.] Chrisman, J. N., 2014: The continuing evolution of dynamic scanning. *NEXRAD Now*, No. 23, NOAA/NWS/Radar Operations Center, Norman, Oklahoma, 8–13, <http://www.roc.noaa.gov/WSR88D/PublicDocs/NNOW/NNow23a.pdf>.
- [9.] Chrisman, J. N., 2016: Mid-volume rescan of low-level elevations (MRLE): A new approach to enhance sampling of quasi-linear convective systems (QLCSs). New Radar Technologies web page, NOAA/NWS/Radar Operations Center, Norman, OK, 21 pp., [https://www.roc.noaa.gov/WSR88D/PublicDocs/NewTechnology/DQ\\_QLCS\\_MRLE\\_June\\_2016.pdf](https://www.roc.noaa.gov/WSR88D/PublicDocs/NewTechnology/DQ_QLCS_MRLE_June_2016.pdf).
- [10.] Conover, W. J., 1999: *Practical Nonparametric Statistics*, 3<sup>rd</sup> Ed. John Wiley & Sons, Inc., New York, NY, 595 pp.

- [11.] Dasey, T. J., M. L. Pawlak, M. A. Isaminger, and M. F. Donovan, 1996: Comparison of the performance of the Integrated Terminal Weather System (ITWS) and Terminal Doppler Weather Radar (TDWR) microburst detection algorithms. In *Workshop on W and Wind Shear Alert Systems*, Oklahoma City, OK, Amer. Meteor. Soc., 53–62.
- [12.] Evans, J. E., and D. M. Bernella, 1994: Supporting the deployment of the Terminal Doppler Weather Radar (TDWR). *Linc. Lab. J.*, **7**, 379–398, <https://www.ll.mit.edu/sites/default/files/publication/doc/supporting-deployment-terminal-doppler-weather-evans-ja-7196.pdf>.
- [13.] Evans, J. E., and E. R. Ducot, 1994: The integrated terminal weather system (ITWS). *Linc. Lab. J.*, **7**, 449–474, [https://www.ll.mit.edu/sites/default/files/publication/doc/integrated-terminal-weather-system-\(itws\)-evans-ja-7203.pdf](https://www.ll.mit.edu/sites/default/files/publication/doc/integrated-terminal-weather-system-(itws)-evans-ja-7203.pdf).
- [14.] Evans, J., and D. Turnbull, 1989: Development of an automated windshear detection system using Doppler weather radar. *Proc. IEEE*, **77**, 1661–1673, <https://doi.org/10.1109/5.47729>.
- [15.] FAA, 1987: System requirements statement for the Terminal Doppler Weather Radar system. Order 1812.9, Federal Aviation Administration, Department of Transportation, Washington, DC, 12 pp., <https://www.faa.gov/documentLibrary/media/Order/1812.9.pdf>.
- [16.] FAA, 1995: Operational requirements document for the Integrated Terminal Weather System (ITWS). Federal Aviation Administration, Department of Transportation, Washington, DC, 40 pp.
- [17.] FAA, 2009: Performance specification: Weather Systems Processor (WSP). FAA-E-2917a, The Wind Shear and Weather Radar Integrated Product Team (AND-420), Federal Aviation Administration, Department of Transportation, Washington, DC, 84 pp.
- [18.] Gatt, P., K. Barr, and M. Margulis, 2015: WindTracer® evolution and recent measurement results. In *Applications of Lasers for Sensing and Free Space Communications*, OSA Technical Digest (online), Optica Publishing Group, LT3D-2, <https://opg.optica.org/abstract.cfm?uri=LSC-2015-LT3D.2>.
- [19.] Hallowell, R. G., 1993: Dual-Doppler measurements of microburst outflow strength asymmetry. In *26<sup>th</sup> Int. Conf. on Radar Meteorology*, Norman, OK, Amer. Meteor. Soc., 664–666.
- [20.] Hallowell, R. G., J. Y. N. Cho, S. Huang, M. E. Weber, G. Paull, and T. Murphy, 2009: Wind-shear system cost benefit analysis update. Project Rep. ATC-341, MIT Lincoln Laboratory, Lexington, MA, 186 pp., [https://www.ll.mit.edu/sites/default/files/publication/doc/2018-12/Hallowell\\_2009\\_ATC-341\\_WW-17238.pdf](https://www.ll.mit.edu/sites/default/files/publication/doc/2018-12/Hallowell_2009_ATC-341_WW-17238.pdf).
- [21.] Hjelmfelt, M. R., 1988: Structure and life cycle of microburst outflows observed in Colorado. *J. Appl. Meteor. Climatol.*, **27**, 900–927, [https://doi.org/10.1175/1520-0450\(1988\)027%3C0900:SALCOM%3E2.0.CO;2](https://doi.org/10.1175/1520-0450(1988)027%3C0900:SALCOM%3E2.0.CO;2).

- [22.] Isaminger, M. A., B. A. Crowe, and E. A. Proseus, 2000: ITWS and ITWS/LLWAS-NE runway alert performance at Dallas-Ft. Worth and Orlando. In *9<sup>th</sup> Conf. on Aviation, Range, and Aerospace Meteorology*, Orlando, FL, Amer. Meteor. Soc., 590–595.
- [23.] Klinge-Wilson, D. L., 1995: Integrated Terminal Weather System (ITWS) demonstration and validation operational test and evaluation. Project Rep. ATC-234, MIT Lincoln Laboratory, Lexington, MA, 112 pp., [https://www.ll.mit.edu/sites/default/files/publication/doc/2018-12/Klinge-Wilson\\_1995\\_ATC-234\\_WW-15318.pdf](https://www.ll.mit.edu/sites/default/files/publication/doc/2018-12/Klinge-Wilson_1995_ATC-234_WW-15318.pdf).
- [24.] Kuster, C. M., and co-authors, 2021: Using  $K_{DP}$  cores as a downburst precursor signature. *Wea. Forecasting*, **36**, 1183–1198, <https://doi.org/10.1175/WAF-D-21-0005.1>.
- [25.] Leone, D. A., R. M. Endlich, J. Petričeks, R. T. H. Collis, and J. R. Porter, 1989: Meteorological considerations used in planning the NEXRAD network. *Bull. Amer. Meteor. Soc.*, **70**, 4–13, [https://doi.org/10.1175/1520-0477\(1989\)070%3C0004:MCUIPT%3E2.0.CO;2](https://doi.org/10.1175/1520-0477(1989)070%3C0004:MCUIPT%3E2.0.CO;2).
- [26.] Martin Marietta, 1994: Wind shear systems cost-benefit and deployment study: System engineering and integration contract for implementation of the National Airspace System plan. ATC-92-1201, Martin Marietta Air Traffic Systems, 91 pp.
- [27.] McCarthy, J., R. Serafin, J. Wilson, J. Evans, C. Kessinger, and W. P. Mahoney, III, 2022: Addressing the microburst threat to aviation: Research-to-operations success story. *Bull. Amer. Meteor. Soc.*, **12**, E2845–E2861, <https://doi.org/10.1175/BAMS-D-22-0038.1>.
- [28.] Michelson, M., W. W. Shrader, and J. G. Wieler, 1990: Terminal Doppler Weather Radar. *Microwave J.*, **33**, 139–148.
- [29.] Newell, O. J., and J. A. Cullen, 1993: ASR-9 microburst detection algorithm. Project Rep. ATC-197, MIT Lincoln Laboratory, Lexington, MA, 71 pp., [https://www.ll.mit.edu/sites/default/files/publication/doc/2018-12/Newell\\_1993\\_ATC-197\\_WW-15318.pdf](https://www.ll.mit.edu/sites/default/files/publication/doc/2018-12/Newell_1993_ATC-197_WW-15318.pdf).
- [30.] NOAA, 2015: NOAA/National Weather Service radar functional requirements. National Weather Service, National Oceanic and Atmospheric Administration, Silver Spring, MD, 57 pp., [https://www.roc.noaa.gov/WSR88D/PublicDocs/NOAA\\_Radar\\_Functional\\_Requirements\\_Final\\_Sept%202015.pdf](https://www.roc.noaa.gov/WSR88D/PublicDocs/NOAA_Radar_Functional_Requirements_Final_Sept%202015.pdf).
- [31.] NOAA, 2022: NOAA radar surveillance requirements: Weather. National Weather Service, National Oceanic and Atmospheric Administration, Silver Spring, MD, January 7, 2022.
- [32.] Pobocikova, I., 2010: Better confidence intervals for a binomial proportion. *Communications—Scientific Letters of the University of Zilina*, **12**, 31–37, <http://komunikacie.uniza.sk/index.php/communications/article/download/897/861/>.
- [33.] ROC, 2008: WSR-88D system specification. Document number 2810000H, code identification 0WY55, WSR-88D Radar Operations Center, Norman, OK, 160 pp.

- [34.] Saltikoff, E., and co-authors, 2016: The threat to weather radars by wireless technology, *Bull. Amer. Meteor. Soc.*, **97**, 1159–1167, <https://doi.org/10.1175/BAMS-D-15-00048.1>.
- [35.] Smalley, D. J., B. J. Bennett, and M. L. Pawlak, 2002: New products for the NEXRAD ORPG to support FAA critical systems. In *19<sup>th</sup> Int. Conf. on Interactive Processing Systems for Meteorology, Oceanography and Hydrology*, Long Beach, CA, Amer. Meteor. Soc., 14.12, <http://ams.confex.com/ams/pdfpapers/57174.pdf>.
- [36.] Smalley, D. J., B. J. Bennett, and R. Frankel, 2005: MIGFA: The Machine Intelligent Gust Front Algorithm for NEXRAD. In *32<sup>nd</sup> Conf. on Radar Meteorology*, Albuquerque, NM, Amer. Meteor. Soc., 8.4, <https://ams.confex.com/ams/pdfpapers/96098.pdf>.
- [37.] Troxel, S. W., and R. L. Delaney, 1994: Machine intelligent approach to automated gust-front detection for Doppler weather radars. In *Proc. Vol. 2220, Sensing, Imaging, and Vision for Control and Guidance of Aerospace Vehicles*, Orlando, FL, SPIE, <https://doi.org/10.1117/12.179602>.
- [38.] Veillette, M. S., B. J. Bennett, M. Pawlak, and R. S. Frankel, 2013: Microburst detection with NEXRAD AMDA. In *36<sup>th</sup> Conf. on Radar Meteorology*, Breckenridge, CO, Amer. Meteor. Soc., 15.315, [https://ams.confex.com/ams/36Radar/webprogram/Manuscript/Paper228790/2013\\_09-16\\_AMS\\_Radar\\_Conf\\_Veillette\\_Final.pdf](https://ams.confex.com/ams/36Radar/webprogram/Manuscript/Paper228790/2013_09-16_AMS_Radar_Conf_Veillette_Final.pdf).
- [39.] Wang, L., Y. Liu, and D. Su, 2019: Wind shear detection algorithm verified using cases from NEXRAD. In *2019 Int. Conf. on Meteorology Observations (ICMO)*, Chengdu, China, IEEE, 1–5, <https://doi.org/10.1109/ICMO49322.2019.9026072>.
- [40.] Weber, M. E., and M. L. Stone, 1994: Low altitude wind shear detection using airport surveillance radars. In *1994 IEEE National Radar Conf.*, Atlanta, GA, IEEE, 52–57, <https://doi.org/10.1109/NRC.1994.328097>.
- [41.] Weber, M. E., J. Y. N. Cho, H. G. Thomas, and J. M. Kurdzo, 2023: An integrated future U.S. weather radar architecture for aviation. *Advances in Weather Radar, Vol. 1*, V. N. Bringi, K. V. Mishra, and M. Thurai, Eds., IET Press, Stevenage, U.K. (in press).
- [42.] Wilson, E. B., 1927: Probable inference, the law of succession, and statistical inference. *J. Amer. Stat. Assoc.*, **22**, 209–212, <https://doi.org/10.1080/01621459.1927.10502953>.
- [43.] Wilson, F. W., and R. H. Gramzow, 1991: The redesigned Low Level Wind Shear Alert System. In *4<sup>th</sup> Int. Conf. on Aviation Weather Systems*, Paris, France, Amer. Meteor. Soc., 370.